

This is the accepted manuscript made available via CHORUS. The article has been published as:

Ferroelectricity in $d^{\{0\}}$ double perovskite fluoroscandates

Nenian Charles and James M. Rondinelli

Phys. Rev. B **92**, 054111 — Published 27 August 2015

DOI: [10.1103/PhysRevB.92.054111](https://doi.org/10.1103/PhysRevB.92.054111)

Ferroelectricity in d^0 double perovskite fluoroscandates

Nenian Charles^{1,*} and James M. Rondinelli^{2,†}

¹Department of Materials Science & Engineering, Drexel University, Philadelphia, PA 19104, USA

²Department of Materials Science & Engineering, Northwestern University, Evanston, IL 60208, USA

(Dated: August 13, 2015)

Ferroelectricity in strain-free and strained double perovskite fluorides, Na_3ScF_6 and K_2NaScF_6 , is investigated using first-principles density functional theory. Although the experimental room temperature crystal structures of these fluoroscandates are centrosymmetric, *i.e.*, Na_3ScF_6 ($P2_1/n$) and K_2NaScF_6 ($Fm\bar{3}m$), lattice dynamical calculations reveal that soft polar instabilities exist in each prototypical cubic phases and that the modes harden as the tolerance factor approaches unity. Thus, the double fluoroperovskites bear some similarities to ABO_3 perovskite oxides; however, in contrast, these fluorides exhibit large acentric displacements of alkali metal cations (Na, K) rather than polar displacements of the transition metal cations. Biaxial strain investigations of the centrosymmetric and polar Na_3ScF_6 and K_2NaScF_6 phases reveal that the paraelectric structures are favored under compressive strain whereas polar structures with in-plane electric polarizations ($\sim 5\text{--}18 \mu\text{C cm}^{-2}$) are realized at sufficiently large tensile strains. The electric polarization and stability of the polar structures for both chemistries are found to be further enhanced and stabilized by a coexisting single octahedral tilt system. Our results suggest that polar double perovskite fluorides may be realized by suppression of octahedral rotations about more than one Cartesian axis; structures exhibiting in- or out-of-phase octahedral rotations about the c -axis are more susceptible to polar symmetries.

PACS numbers: 31.15.A-, 77.80.-e

I. INTRODUCTION

Many twenty-first century technologies such as lasers, sensors, transistors, and non-volatile recording media depend on materials without spatial inversion symmetry.^{1–4} However, noncentrosymmetric compounds occur infrequently in nature, particularly in solid-state inorganic materials where they comprise less than $\sim 18\%$ of all known materials.^{5–8} One way to overcome the limited material availability is to elucidate the forces favoring noncentrosymmetric distortions, and then use that understanding to design, for example, new ferroelectric materials with polar atomic displacements.

Within this context, one of most studied crystal families for realizing new polar materials are oxide perovskites with chemical formula ABO_3 owing to the perovskite structure's chemical and structural flexibility.^{5,9} Although there remains an incomplete chemical recipe for the design of new polar perovskites, research in ternary transition metal oxides have successfully identified key atomic and electronic structure features that reliably describe the tendency for a given composition to be polar and ferroelectric: Octahedral rotations and antipolar displacements of the 12-fold coordinated A -site cations may suppress ferroelectricity,^{10,11} and thus they need to be deactivated. Prior work has established that for ordered perovskites, for example, $(\text{AA}')\text{BO}_3$, polar displacements can stabilize polar structures in A -site driven ferroelectric perovskites;^{12,13} however, the magnitude of the polar displacements is often small in the absence of covalent interactions. Furthermore, larger polarizations are obtained in ABO_3 perovskites by incorporating stereo-active (ns^2np^0) cations on the A -site or d^0 transition metal cations on the B -site, which stabilize polar distortions by increasing

covalent interaction between the metal-ligand framework through the second order Jahn-Teller effect (SOJT).^{9,14–16}

Although these operating principles are useful for perovskite *oxides*, the guideline are not universal across all anion chemistries in structures characterized by metal-anion octahedra with different covalency and polarizability.¹⁷ Intriguingly, inversion symmetry lifting distortions are more scarce in the more ionic fluoroperovskites (ABF_3) than in oxides,¹⁸ despite polar phases commonly appearing in fluorides belonging to the ABF_4 , ABF_5 , $\text{A}_5\text{B}_3\text{F}_{19}$ and $\text{A}_3\text{B}_5\text{F}_{15}$ families.^{17,19,20} Two specific centrosymmetric transition metal (M) double perovskite fluorides (A_2BMF_6) include those belonging to the cryolite and elpasolite crystal families (Fig. 1): Elpasolites with the chemical formula A_2BMF_6 are usually cubic, $Fm\bar{3}m$ symmetry without any octahedral rotations ($a^0a^0a^0$). Cryolite fluorides, A_3MF_6 , where $B = A$, are distorted and frequently crystallize in $P2_1/n$ symmetry with the Glazer tilt system $a^-a^-c^+$.²¹ These observations leads us to pose the question: Are octahedral rotations or increased ionicity in perovskite fluorides responsible for the suppression of ferroelectricity? Also, given the possibility for thin film growth of fluorides,^{22–25} we propose a related challenge: Can polar phases be stabilized in fluoroperovskites with epitaxial strains as is achieved in oxides?^{26–28}

In this work, we use first principles calculations to examine the lattice dynamics of the cryolite Na_3ScF_6 ($P2_1/n$)^{31,32} and elpasolite K_2NaScF_6 ($Fm\bar{3}m$).^{33,34} We find that the low-frequency polar IR-active phonons in these double perovskite fluorides are dominated by the displacements of alkali metals (K and Na) with smaller accompanying displacements of the Sc^{3+} ion. Similar to ABO_3 perovskites, the frequency of the polar modes harden with increasing tolerance factor, t .¹¹ Specifically,

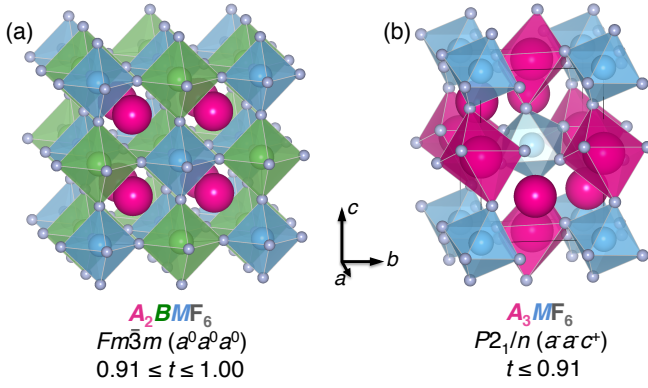


FIG. 1. Common structure types adopted by double perovskite fluorides. Elpasolites (a) have stoichiometry A_2BMF_6 and are typically found in cubic $Fm\bar{3}m$ symmetry. Cryolites (b) have stoichiometry A_3MF_6 and often crystallize in a rotationally-distorted monoclinic $P2_1/n$ symmetry. In cryolites the 12-fold coordinated A cation is chemically identical to the octahedrally coordinated B -site cation ($A = B$). The structure stability range for the each family within the given symmetry is specified by the tolerance factor, t , obtained using Shannon radii.^{29,30}

we find a ferroelectric instability at the equilibrium unit cell volume for the high symmetry cubic structure of Na_3ScF_6 (with the smaller A -site cation) whereas in K_2NaScF_6 the polar mode is hard. Our analyses indicate that the driving force for the ferroelectric instability and octahedral rotations are identical, *i.e.*, owing to underbonding of the A -site cation.¹³

We also investigate the strain dependence of the polar phase stabilities compared to the centrosymmetric ground state structure in Na_3ScF_6 and K_2NaScF_6 and uncover that compressive strain favors centric geometries. However, we observe that tensile strain couples strongly to the polar instability, favoring displacements in the ab plane that stabilize lower symmetry polar structures over the bulk centric phases. For the polar structures, we compute the electric polarizations and find that they vary from ~ 5 – $18 \mu C cm^{-2}$ in the ab plane for Na_3ScF_6 and K_2NaScF_6 over the tensile strain range explored. The origin for the polar displacements is due to an increase in the metal-fluoride bond lengths from the strain, which destabilizes the A cation bond geometry. Thus, stable polar geometries result from the acentric distortions that optimize the bond distances in the metal-ligand framework.

II. COMPUTATIONAL DETAILS

We performed density functional theory (DFT) calculations with the general gradient approximation (GGA) of Perdew-Burke-Ernzerhof revised for solids³⁵ (PBEsol) as implemented in the Vienna *Ab initio* Simulation Package (VASP)^{36,37} with the projector augmented wave (PAW) method³⁸ to treat the core and valence electrons using the following valence configurations: $2p^63s^1$ for Na, $3p^64s^13d^2$ for Sc, and $2s^22p^5$ for F. We use a $7 \times 7 \times 7$ Monkhorst-Pack

k -point mesh³⁹ with Gaussian smearing (10 meV width) for Brillouin zone (BZ) integrations and a 600 eV plane wave cutoff. Structural relaxations are performed until the Hellmann-Feynman forces are less than $1 meV \text{ \AA}^{-1}$ on each atom. We use density-functional perturbation theory to compute the lattice phonons of Na_3ScF_6 and K_2NaScF_6 in the ideal cubic structure, $Fm\bar{3}m$. Owing to the large unit cell size (40 atoms), all phonon calculations are performed on a $\sqrt{2} \times \sqrt{2} \times \sqrt{2}$ supercells. The phonon mode symmetries are analyzed using the PHONOPY package.⁴⁰

III. RESULTS

A. Na_3ScF_6 Lattice Dynamical Properties and Low Energy Structures

Na_3ScF_6 crystallizes in the common cryolite symmetry, *i.e.*, $P2_1/n$ and $a^-a^-c^+$ tilt pattern, with a tolerance factor $t = 0.87$.³¹ With this in mind, we first examine the tendency to ferroelectricity by exploring the phonon frequencies of the ideal cubic phase and considering how combinations of soft modes responsible for the monoclinic symmetry support or suppress polar displacements. We find a ferroelectric lattice instability transforming as the irreducible representation (irrep) Γ_4^- ($I4mm$) with a frequency of $102i cm^{-1}$. Fig. 2(a) shows the polar mode mainly consists of displacements of the 12-fold coordinate Na ions and fluoride anions, similar to what has been recently reported for ABF_3 perovskites.²³ The character of the polar mode in Na_3ScF_6 is distinct from that commonly observed in perovskite oxides, whereby the 6-coordinate transition metal and oxide anions undergo polar displacements.¹¹ Given that the polar mode found in Na_3ScF_6 is dominated by A -site displacements, the origin of the the polar instability is unlikely to originate from a SOJT mechanism.

Next, we find the mode frequencies for the unstable ScF_6 tilt modes are more unstable than the polar mode. The in-phase $a^0a^0c^+$ rotation described by X_3^+ has a mode frequency of $\nu = 133i cm^{-1}$ [Fig. 2(b)] and the out-of-phase $a^-a^-c^0$ rotation [(Γ_4^+) , Fig. 2(c)] has a mode frequency of $\nu = 135i cm^{-1}$. Condensing the in-phase and out-of-phase distortions into the $Fm\bar{3}m$ aristotype produces the centrosymmetric $P4/mnc$ and $C2/m$ structures, respectively.

To investigate the relative stabilities of structures derived from the unstable lattice modes, we freeze-in each distortion mode into the ideal cubic phase and then perform full volume and atomic relaxations. We find that although the polar $I4mm$ structure is energetically more stable than the $Fm\bar{3}m$ phase by 263 meV/f.u. (Table I), the phases containing octahedral rotations are always more energetically favorable. Indeed the monoclinic $P2_1/n$ structure, which contains coexisting $a^0a^0c^+$ and $a^-a^-c^0$ rotations, is most stable ($a^-a^-c^+$). Furthermore, we find that the sum of the relative energy gain ΔE (and rotation

TABLE I. Structural and energetic comparison for equilibrium Na_3ScF_6 phases in space group symmetries obtained by condensing unstable lattice modes with frequencies, ν . The interaxial angles for all DFT-PBEsol structures were constrained to $\alpha = \beta = \gamma = 90^\circ$ except for the ground state $P2_1/n$ phase, where $\beta = 90.72^\circ$ is fixed to the experimentally reported monoclinic angle.³¹ Relative energies differences per formula unit (f.u.), ΔE , are reported with respect to the aristotype $Fm\bar{3}m$ structure.

Symmetry	Glazer tilt	Mode	ν (cm^{-1})	Lattice constants (\AA)	ΔE (meV/f.u.)	Rotation angle ($^\circ$)
$Fm\bar{3}m$	$a^0a^0a^0$	—	—	8.306 ($a = b = c$)	0	0.0
$I4mm$	$a^0a^0a^0$	Γ_4^- [001]	102i	5.942 ($a = b$), 8.404 (c)	-263	0.0
$P4/mnc$	$a^0a^0c^+$	X_3^+ [001]	133i	5.795 ($a = b$), 8.196 (c)	-576	18.5
$C2/m$	$a^-a^-c^0$	Γ_4^+ [110]	135i	5.657 (a), 5.865 (b), 8.147 (c)	-926	21.9
$P2_1/n$	$a^-a^-c^+$	$X_3^+ \oplus \Gamma_4^+$	—	5.588 (a), 5.794 (b), 8.105 (c)	-1050	13.0, 21.8

angle amplitudes) obtained from the in-phase and out-of-phase rotations independent of any other distortions is greater than that computed for the ground state structure (Table I). This result indicates that the coexisting in-phase and out-of-phase rotations in $P2_1/n$ compete with each other.

We now investigate whether the polar mode displacements are compatible with the single-tilt structures exhibiting the $a^0a^0c^+$ and $a^-a^-c^0$ octahedral rotations. We begin by computing the zone-center phonons for each relaxed intermediate $P4/mnc$ and $C2/m$ structure given in Table I. We find in the $P4/mnc$ phase that the softest mode, $\nu = 118i \text{ cm}^{-1}$, describes out-of-phase ScF_6 octahedral rotations and transforms like Γ_4^- .⁴² Condensation of the mode would drive the $P4/mnc \rightarrow P2_1/n$ symmetry reduction. Interestingly, we also find that a polar instability is present at $\nu = 82i \text{ cm}^{-1}$ with Γ_4^- symmetry. Here, Na and F displacements along the [110] direction would produce a polar $P4/mnc \rightarrow Pm$ transition. Hence, in-phase rotations alone in Na_3ScF_6 do not appear to suppress the polar instability, which is consistent with that reported for perovskite oxides,¹¹ i.e., the frequencies of the soft ferroelectric modes decrease but remain unstable in the presence of the $a^0a^0c^+$ tilt. On the other hand, the

intermediate $C2/m$ structure with tilt pattern $a^-a^-c^0$ does not have a polar instability. $C2/m$ has one unstable phonon, $\nu = 66i \text{ cm}^{-1}$ that produces the centrosymmetric $C2/m \rightarrow P2_1/n$ transition.

B. Strain Effects on Na_3ScF_6 Structure Stability

Here we examine how biaxial strain affects the stability and local structure of the various Na_3ScF_6 phases. For all structures, we assume epitaxy occurs on a cubic substrate that forces the in-plane lattice parameters to be equal ($a = b$). At a value of 0% strain, we set the pseudocubic lattice constant of the substrate $a_S = (a + b)/2$, where a and b are the bulk equilibrium lattice constants of the phase being considered (see Table I).⁴³ At each strain state, the c axis and atomic positions are relaxed until the forces and stresses are below the specified threshold.

Fig. 3(a) shows the evolution in the total energy of Na_3ScF_6 as a function of biaxial strain for the ground state $P2_1/n$ ($a^-a^-c^+$ tilt) and low-energy polar $I4mm$ structure without octahedral rotations ($a^0a^0c^0$ tilt). We observe that at 0% strain the monoclinic phase is $\sim 0.7 \text{ eV/f.u.}$ more stable than the polar structure. We find that increasing compressive (negative) or tensile (positive) strain leads to an increase in the energy of both phases. Nonetheless, the energy difference between $P2_1/n$ and $I4mm$ is always greater than 0.5 eV [Fig. 3(b)], and the energy difference in the tensile range also becomes approximately strain-independent. These results indicate that epitaxial strain is ineffective at stabilizing the polar, rotation-free, structure over the monoclinic phase with octahedral rotations.

We next investigate the effect of in-plane epitaxial strain on the phase stability of the two intermediate, $P4/mnc$ and Pm , phases [Fig. 4(a)]. We find that at 0% biaxial strain the Pm phase is more favorable than the centrosymmetric $P4/mnc$ intermediate. The ground state $P2_1/n$ ($a^-a^-c^+$) structure is $\sim 0.47 \text{ eV/f.u.}$ more stable than the polar Pm structure. We also observe that compressive strain increases the total energy of all Na_3ScF_6 structures. For strains greater than -2% strain, we find that the Pm phase with the polar displacements is destabilized relative to the non-polar $P4/mnc$ structure. In contrast, for increasing tensile strain this stability reversal among the

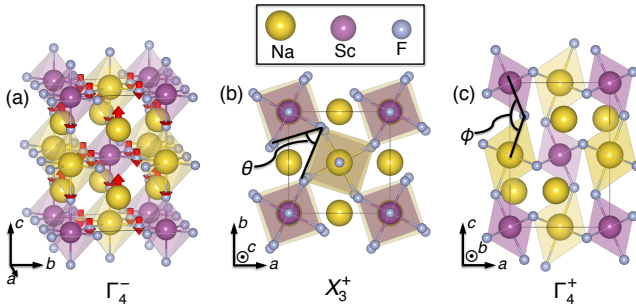


FIG. 2. Unstable lattice distortions at Γ and X for Na_3ScF_6 . (a) Γ_4^- is a polar displacement of A-site Na atoms and F atoms in the [001] direction indicated by the direction of the red arrows; the length indicates the relative magnitude of the displacement for the ions. (b) X_3^+ is an in-phase octahedral rotation about the [001] axis. The rotation angle is measured as $(90 - \theta)/2$. (c) Γ_4^+ is an out-of-phase rotation of octahedra about the [110] direction. The tilt angle is measured as $(180 - \phi)/2$. These modes may be visualized using the resources in Ref. 41.

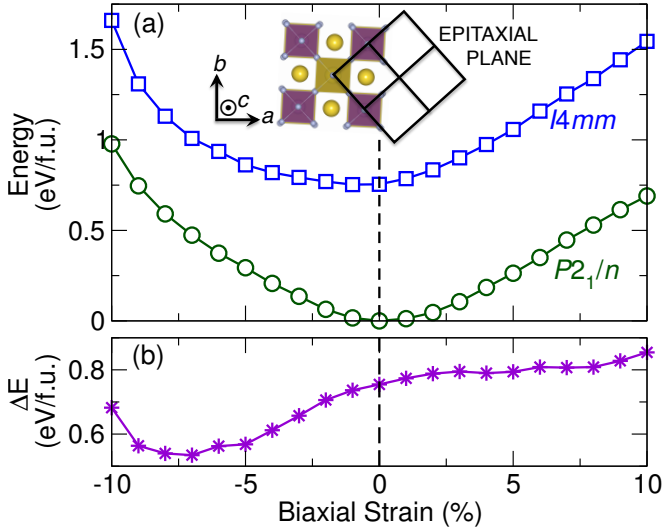


FIG. 3. (a) Stability of the monoclinic $P2_1/n$ ground state (circles) and polar $I4mm$ (squares) structure with epitaxial strain. The inset shows a schematic of the epitaxial relationship between Na_3ScF_6 and the cubic substrate. (b) The energy difference between the structures is obtained as $\Delta E = E(I4mm) - E(P2_1/n)$.

two low-energy phases with only in-phase tilts does not occur: The Pm phase is always more stable than the $P4/mnc$ structure with a single octahedral tilt and no polar distortion.

Remarkably, for sufficiently large tensile strains ($> 8\%$) we find it possible to stabilize the polar Pm structure relative to the bulk $P2_1/n$ ground state. With increasing compressive or tensile strain the total energy for both centrosymmetric structures ($P4/mnc$ and $P2_1/n$) evolve in a similar fashion. In the tensile region, however, the total energy for the polar Pm phase initially increases for small strains between $\sim 4\%$ and then the curvature above this value changes such that the energy difference between the $P2_1/n$ and Pm phases decreases.

We next apply mode-crystallography analyses⁴⁴ to the Pm structures to understand this strain-dependent phase stability: The Pm phase is characterized by three main structural distortions, *i.e.*, in-phase rotations about the $[001]$ direction (X_3^+), polar displacements (Γ_4^-), and antipolar displacements (X_5^-).⁴¹ We observe that the amplitude of the in-phase rotation remains fairly constant below $+4\%$ strain [Fig. 4(b)]. However, the rate at which the amplitude of the polar mode changes with strain increases or strains $\geq 4\%$. By comparing the evolution of the electric polarization in the ab plane, shown in Fig. 4(c), with the amplitude of the rotation mode, we find similar strain-dependent behavior, including a marked increase in polarization near 4% strain. In contrast, the evolution of the antipolar mode amplitude shows no significant changes about 4% strain; it evolves in an nearly linear fashion.⁴¹

To understand the nature of the strain interactions on the Pm phase, we next examine in detail the energetic de-

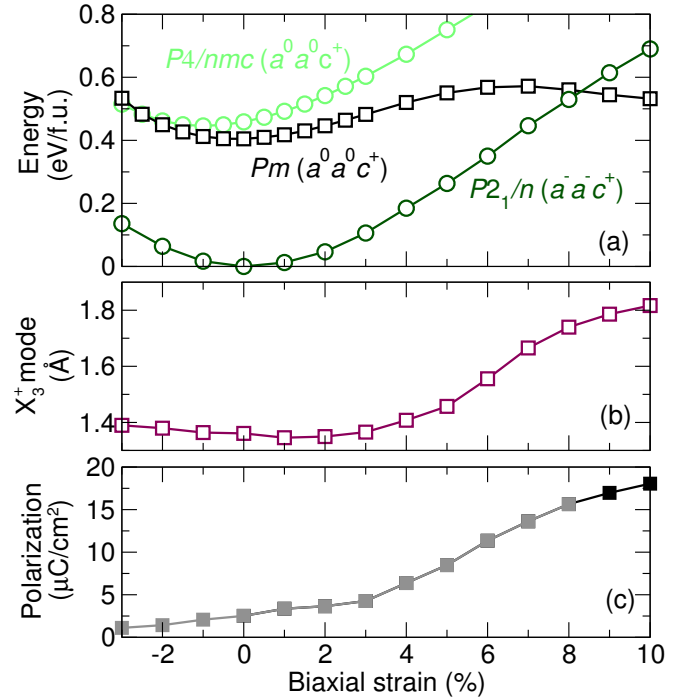


FIG. 4. (a) Total energy evolution with biaxial strain for low-energy Na_3ScF_6 polymorphs. The evolution in the (b) in-phase rotation mode amplitude and (c) electric polarization for the Pm phase with strain. The gray line in (c) indicates the region where the polarization is in accessible at 0 K.

pendence of the three coexisting Γ_4^- , X_3^+ and X_5^- modes at 4% strain. Fig. 5(a)-(c) show that at this value of tensile strain, the Γ_4^- mode, which produces a Cm symmetry [see panel (d)], is an energy-raising distortion in the absence of coupling to any other mode (see the 0% curves in all panels). Next we consider the coupling of the polar mode to another distortion at a finite fraction for which the latter is present in the equilibrium strained structure, indicated by the percentage labels. When the polar mode is coupled to finite amplitudes of the in-phase rotation or the anti-polar distortion at 4% tensile strain [Fig. 5(a) and (b)], we observe that these polar Pm phases are further unfavored. Fig. 5(c) shows that for fixed amplitudes of $X_3^+ \oplus X_5^-$ coupled to Γ_4^- ; however, there is a net energy gain that increases with the amplitude of the coexisting rotation and anti-polar displacements. We conclude then for Na_3ScF_6 that in-plane tensile strain favors the stabilization of a polar structure via cooperative coupling of the in-phase rotations and antipolar displacements to the polar mode.

We note that for Na_3ScF_6 the 9% in-plane tensile strain (pseudocubic, $a_S \approx 4.46 \text{ \AA}$) needed to stabilize the Pm phase over the $P2_1/n$, however, exceeds the pseudocubic lattice constants of available substrates.⁴⁵ Thus, although tensile strain favors polar distortions in the cryolite double perovskite, the energetic gain arising from the octahedral rotations is more favorable at most accessible strain values and would lead to centric fluorides. Therefore, we propose

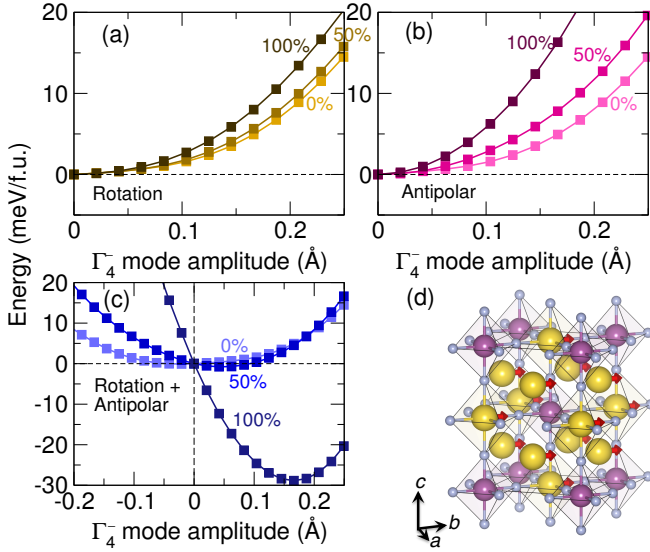


FIG. 5. Energetic dependence of various mode distortions at 4% biaxial strain for Na_3ScF_6 . Coupling between Γ_4^- and fixed amplitudes of (a) the in-phase rotation, X_3^+ , (b) the antipolar distortion, X_5^- , and (c) the linear combination of the two modes, $X_3^+ \oplus X_5^-$, at 0% strain. (d) The polar displacements of ions in the Γ_4^- mode. The normalized energy gains are obtained by increasing the amplitudes of the in-phase and antipolar distortions at fixed percentages found in the equilibrium structure at 4% tensile strain.

the use of biaxial strain in a fluoroperovskite that is free of octahedral rotations in its ground state. In this way, one would not be required to overcome the large stability provided by the octahedral rotations to the total energy. We explore such a scenario in the next section.

C. Bulk and Thin Film K_2NaScF_6

Chemical substitution allows one to exploit steric effects in double perovskite fluorides. The replacement of Na cations on the A-site of Na_3ScF_6 by a larger alkali metal would give an elpasolite (A_2NaScF_6) with significantly less underbonding of the A cation. The larger A-site cation would therefore reduce the tendency towards octahedral rotations, which would be reflected in a larger tolerance factor. We conjecture this type of chemical substitution may provide a promising avenue for stabilizing polar phases at smaller pseudo-cubic lattice constants by eliminating competing (rotational) distortions.

To test our hypothesis, we investigate the chemistry K_2NaScF_6 ($t = 0.954$), which is experimentally reported to be a cubic double perovskite fluoride at room temperature ($Fm\bar{3}m$, $a = 8.47$ Å).³⁴ We first examine the dynamical stability of K_2NaScF_6 by performing phonon calculations on the PBEsol relaxed equilibrium cubic structure. For our calculations, we find the triply degenerate polar Γ_4^- modes are hard with $\nu = 130$ cm^{-1} , corresponding to displacements along either [001] or [110].

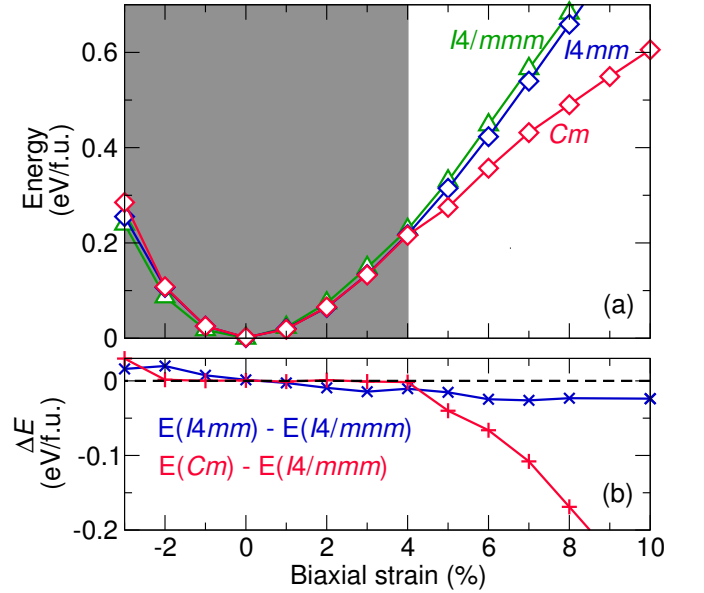


FIG. 6. Evolution of the (a) relative total energy and (b) energy differences (ΔE) with biaxial strain for low-energy polar phases of K_2NaScF_6 with respect to the equilibrium centrosymmetric ($I4/mmm$) structure. In (a) the area shaded gray represents the biaxial strain region over which the centrosymmetric phase is stable.

Given the sensitivity of ferroelectric modes to pressure^{10,46} and the tendency of Na_3ScF_6 to prefer polar displacements at large tensile strains, we next examine the pressure dependence of these polar modes in K_2NaScF_6 at unit cell volumes greater than the equilibrium volume. This computational experiment corresponds to a negative pressure configuration. Upon increasing the equilibrium cubic lattice constant by 5%, we find unstable zone center modes ($45i$ cm^{-1}) that are also three-fold degenerate with Γ_4^- symmetry. Similar to Na_3ScF_6 , the Γ_4^- [001] mode drives the $Fm\bar{3}m \rightarrow I4mm$ symmetry reduction whereas the Γ_4^- [110] mode governs the $Fm\bar{3}m \rightarrow Cm$ transition. All atoms contribute to this mode with displacements along the [001] and [110] directions, respectively.⁴¹

Now we investigate the stability of the polar $I4mm$ and Cm phases relative to the cubic structure with biaxial strain (Fig. 6). Note that the centrosymmetric cubic symmetry of the bulk phase reduces to tetragonal $I4/mmm$ owing to the mechanical constraint from epitaxy. We find that compressive strain favors the centrosymmetric phase over the polar structures (~ 40 meV/f.u.). Consistent with our negative pressure simulation, Fig. 6(a) shows that increasing tensile strain increases the stability of the polar structures over the centrosymmetric geometry. The energy of the $I4mm$ phase is approximately 20 meV/f.u. or less lower in energy than the $I4/mmm$ structure for tensile strains above 1% [Fig. 6(b)]. In contrast, the relative stability of the Cm phase over the $I4/mmm$ structure increases steadily for strains above 4%. Below this value the polar phases are nearly degenerate with each other. These results show that tensile strain stabilizes polar ionic

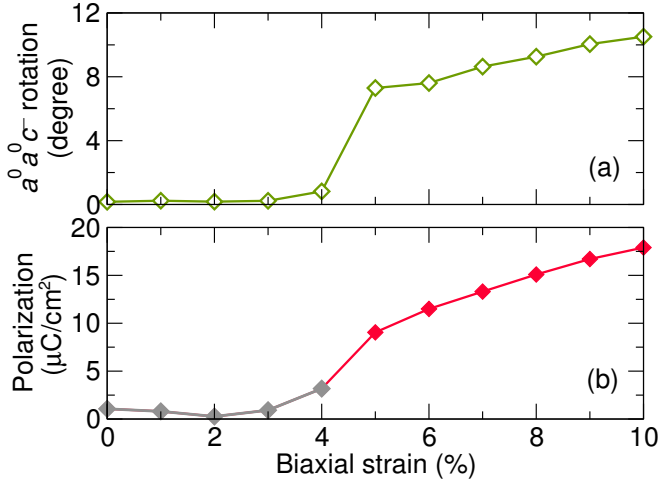


FIG. 7. Evolution of the (a) out-of-phase rotation angle and (b) in-plane electric polarization in Cm K_2NaScF_6 as a function of tensile strain. The gray line represents the region where the polar state is inaccessible.

displacements in the epitaxial plane rather than orthogonal to it. Such coupling of the in-plane polar distortions to tensile strain is consistent with prior work in ABO_3 perovskites.^{28,47,48}

A symmetry mode analysis of K_2NaScF_6 above the 4% critical strain reveals that the Cm equilibrium structure is characterized by three main irreps. First, the polar mode Γ_4^- displaces the K, Na and Sc atoms in the ab plane. The Γ_5^- mode contains polar displacements of F ion along the ab plane. The third main distortion transforms as Γ_4^+ and describes out-of-phase rotations about the c -axis, Glazer tilt system $a^0a^0c^-$.⁴¹

The strain dependence of the out-of-phase rotation mode and Γ_4^- mode amplitudes, which we translate to a rotation angle and electric polarization, are shown in Fig. 7. The stabilization of the Cm phase above 5% strain as shown in Fig. 6 corresponds to the abrupt increase in the out-of-phase rotation angle and enhanced electric polarization (Fig. 7). This indicates that the octahedral rotations may be necessary to stabilize the polar phase. Interestingly, the latter result seemingly contradicts our initial hypothesis of eliminating competing rotational distortions to access polar geometries. However, we note that the polar phase of K_2NaScF_6 , much like Na_3ScF_6 , exhibits a single rotation about the $[001]$ direction.

We next examine the coupling of the out-of-phase rotation modes to the polar modes at 5% strain. We observe that if the octahedral rotations coexist with either polar modes Γ_4^- [Fig. 8(a)] or Γ_5^- [Fig. 8(b)], the energy is always higher and the quadratic dependence of the energy landscape is greater than when the rotations are absent. However, Fig. 8(c) indicates that the $\Gamma_4^- \oplus \Gamma_5^-$ coupling lowers the energy for increasing distortion amplitude, and together these modes give the Cm symmetry. This suggests that the two polar modes must coexist in order to drive the system to a stable polar configuration. Note the

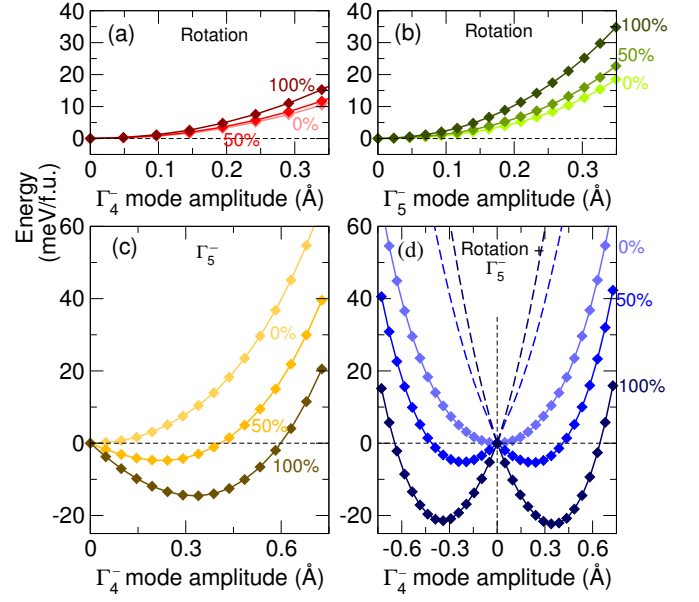


FIG. 8. Evolution in the energy for K_2NaScF_6 as a function of interacting lattice modes at 5% strain. (a) The coupling between the polar Γ_4^- and the out-of-phase rotation Γ_4^+ modes; (b) the polar Γ_5^- and the out-of-phase rotation Γ_4^+ modes; (c) the two polar modes *i.e.*, $\Gamma_4^- \oplus \Gamma_5^-$ (no rotations); and (d) the linear combination of all three modes, $\Gamma_4^- \oplus \Gamma_5^- \oplus \Gamma_4^+$. Here the symmetry equivalent minima are obtained by computing the energy for positive and negative amplitudes of the polar and rotational distortion modes. The normalized energy gains are obtained by increasing the amplitudes of the distortions at fixed percentages found in the equilibrium structure at 5% tensile strain.

combination of any two (Γ_4^- , Γ_5^- , or Γ_4^+) modes will also produce the Cm symmetry. As such all three modes also couple to the lowest order via a trilinear term in the free energy, $E_{\text{trilinear}} \propto \Gamma_4^- \Gamma_5^- \Gamma_4^+$. When all three distortions are combined, *i.e.*, $\Gamma_4^- \oplus \Gamma_5^- \oplus \Gamma_4^+$ [Fig. 8(d)], the polar ground state is further stabilized. However, our results suggest that the Cm phase of K_2NaScF_6 can indeed exist without the out-of-phase rotation. The rotations act to enhance the stability of the ferroelectric phase provided by the biquadratic coupling between the two polar modes [Fig. 8(c)]. This result is distinct from Na_3ScF_6 where the polar phase could not be stabilized in the absence of the in-phase rotation. Moreover, unlike many layered polar perovskites and complex antiferroelectrics,⁴⁹ our results suggest that the trilinear coupling may be less important to the stability of the polar phase.

Here we successfully demonstrate that the critical strain state can be reduced to stabilize a polar polymorph by eliminating the competing out-of-phase $a^-a^-c^0$ rotation mode present in the equilibrium Na_3ScF_6 phase with chemical substitution. Importantly, we note that the large radius of K compared to Na results in larger equilibrium lattice constants for K_2NaScF_6 over Na_3ScF_6 . As a result, the 5% strain state predicted to stabilize the Cm phase of K_2NaScF_6 would require a pseudo-cubic lattice constant of 4.43 Å, which is also beyond that ac-

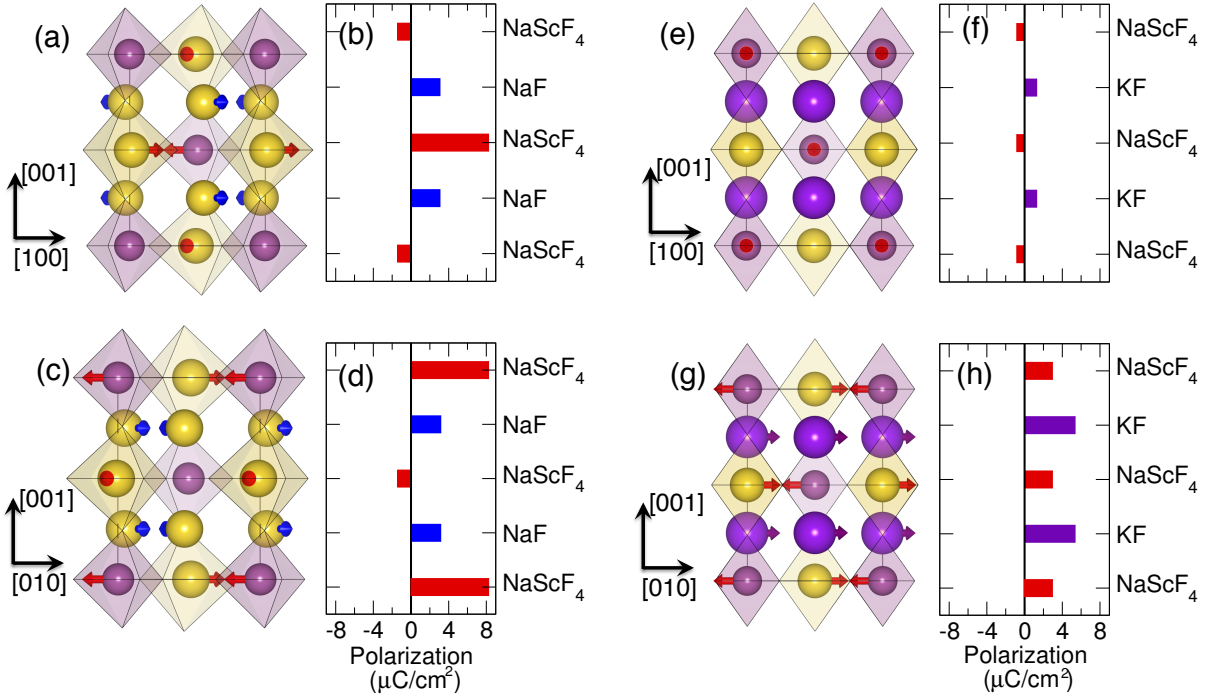


FIG. 9. Layer-resolved polarizations for polar Na_3ScF_6 (Pm) and K_2NaScF_6 (Cm) at 10% tensile strain. (a) The cation displacements and (b) the layer-resolved polarization for Na_3ScF_6 along the $[100]$ direction for Na_3ScF_6 . (c) The cation displacements and (d) the layer-resolved polarization for Na_3ScF_6 along the $[010]$ direction. Similarly, panels (e,f) and (g,h) depict the same information for K_2NaScF_6 along the $[100]$ and $[010]$ directions, respectively. Berry phase calculations result in the total electric polarization for Na_3ScF_6 at 10% to be $P = 12.7\hat{x} + 12.8\hat{y}$, which is close to that obtained by summing the layer dipoles, *i.e.*, $\Sigma p = 13.0\hat{x} + 13.1\hat{y}$. Similarly for K_2NaScF_6 at 10%, $P = 1.4\hat{x} + 17.9\hat{y}$ and $\Sigma p = 0.9\hat{x} + 16.6\hat{y}$.

cessible in commercially available perovskites substrates [$a_S(\text{LaLuO}_3) = 4.17 \text{ \AA}$].⁵⁰ Our analysis suggests that the critical value could be reduced further with alternate chemistries by optimizing the tolerance factor.

IV. DISCUSSION

Ferroelectricity in fluoride perovskites has been speculated for some time. However, to date there have only been a few first principles studies attempting to elucidate routes towards the stabilization of polar phases in fluoride perovskites.^{23,51} Our results show that the structure distortions present in bulk double perovskite fluorides, much like ABO_3 perovskites, are mainly controlled by cation sizes.^{29,52} Although fluoroperovskite structures are also prone to octahedral rotations, polar lattice instabilities may also be present and our lattice dynamical calculations for Na_3ScF_6 ($t = 0.87$) and K_2NaScF_6 ($t = 0.95$) reveal that the ferroelectric mode frequencies harden with increasing tolerance factor. The latter observation has previously been detailed in Ref. 11 for ABO_3 perovskites. However, in contrast to ABO_3 perovskites, the polar displacements in the cryolite and elpasolite fluorides are strongly dominated by displacements of the alkali metals (Na, K) and fluoride ions rather than the 6-coordinate transition metal cations.²³

Our first principles calculations and structural analy-

ses demonstrate that the double perovskites Na_3ScF_6 and K_2NaScF_6 show similarities to strain-activated ferroelectrics.^{23,27,28,53} First, much like low tolerance factor incipient perovskites, the strain-stabilized polar Pm phase of Na_3ScF_6 exhibits octahedral rotations. In simple perovskites without cation order, the acentric geometries have the $a^-a^-c^+$ tilt pattern,^{23,28} but here, the $a^0a^0c^+$ tilt *supports* the polar phase of Na_3ScF_6 . Furthermore, the electric polarization in the ab plane of Na_3ScF_6 is realized by coupling of the polar mode with the in-phase rotation about the c axis. The latter is in contrast to strained CaTiO_3 , where the polarization that appears has little dependence on the amplitude of the rotation modes.²⁸

Second, K_2NaScF_6 is stable in cubic symmetry at room temperature, similar to high tolerance factor incipient ferroelectric SrTiO_3 . Under tensile strain both chemistries demonstrate strain-induced polarizations in the ab plane with coexisting out-of-phase octahedral rotations. For compressive strains K_2NaScF_6 adopts the centrosymmetric phase. SrTiO_3 , on the other hand, shows an enhancement of the polar mode along the $[001]$ direction in the compressive strain region.²⁷ Indeed, experiments have confirmed that strain-induced polar phases of SrTiO_3 can also coexist with antiferrodistortive octahedral rotations at low temperatures.^{53,54} Here we find that the out-of-phase rotation in K_2NaScF_6 may not be pivotal to the stability of the Cm phase, but there is a strong

polarization-rotation coupling that augments the size of the electric polarization.

To better understand the mechanism responsible for the strain-induced polar phases of Na_3ScF_6 and K_2NaScF_6 , we compute the layer resolved-polarization in both structures at 10% tensile strain. **Fig. 9** shows the layer polarizations decomposed along the a and b axes; all layers are found to contribute to the total polarization. These values are in excellent agreement with those obtained with our Berry phase calculations. Interestingly, for Na_3ScF_6 we observe that the polarization from the NaScF_4 layers is about twice that of the NaF layers. This behavior can be understood with the help from **Fig. 9(a)** and our mode coupling investigation (**Fig. 5**). Note that in the NaScF_4 layers, the 6-fold coordinated Na and Sc ions displace in an antipolar fashion with respect to each other. We conjecture that when the antipolar X_5^- and polar Γ_4^- mode couple they act to amplify the off-centering in the NaF_6 octahedra over the more rigid ScF_6 octahedra along the ab direction. The result is a net polarization in the direction of displacement of the Na ion [**Fig. 9(b)**]. Similar behavior is seen in the NaF layers; despite antipolar displacements of the Na ions, the polar mode leads to aligned layer polarizations in the NaF layers. Thus, resulting in a stable polar Na_3ScF_6 structure that has a small A -site contribution to the total polarization [**Fig. 9(b)** and (d)].

Panels (e) through (h) in **Fig. 9** reveal that the polarization in K_2NaScF_6 is dominated by acentric displacements in the KF layers rather than the NaScF_4 layers in the ab plane. From our coupling investigations (**Fig. 8**), we note that the Cm K_2NaScF_6 phase is stabilized by combining two polar modes. We assume that in contrast to Na_3ScF_6 , the absence of the canceling antipolar distortion in K_2NaScF_6 leads to the larger contribution from the A -site cations (K ions) to the total polarization.

The rationale for the stabilization of the polar Na_3ScF_6 and K_2NaScF_6 phases at large tensile strain can be understood from bond valence arguments.⁵⁵ Increasing tensile strain leads to lattice deformations that stretch the metal-ligand bond network. Cations that sit at a center of a cavity that is too large will have a low bond valence sum. To recover the preferred valence the metal-ligand framework is optimized by compensating lattice distortions.^{15,55} In these materials, the off-centering of the metal ions and the octahedral rotations are the lattice responses that improve the under coordinated bond environments.

V. CONCLUSION

We performed a first principles study based on density functional theory to understand the competition between polar and non-polar lattice instabilities in double perovskite fluorides. We explored the feasibility of using strain engineering to stabilize polar polymorphs over centrosymmetric phases in Na_3ScF_6 and K_2NaScF_6 .

From our analysis of the polar displacements in Na_3ScF_6 and K_2NaScF_6 , we find that the primary contributors are the alkali metals (K, Na) and F ions. The ferroelectric modes computed at the equilibrium cubic volumes result in unstable modes in Na_3ScF_6 but stable modes for K_2NaScF_6 . The softening of the ferroelectric modes with negative hydrostatic pressure in K_2NaScF_6 thus suggests that the polar instability is driven by increasing the under-bonding between the A -site cation and the ligand.¹³ This indicates that the same structural mechanism controls the tendency towards rotational instabilities and A -site dominant polar instabilities in Na_3ScF_6 and K_2NaScF_6 .

In both chemistries, large tensile strains stabilize polar geometries that couple strongly to a single rotational distortion about the c axis ($a^0a^0c^+$ or $a^0a^0c^-$). Our results imply that in the double perovskite fluorides, one may only need to suppress the two-tilt out-of-phase rotation, $a^-a^-c^0$, to tip the balance towards polar structures. Although thin film growth of fluorides has been successful using molecular beam epitaxy,^{22,25} our predicted polar phases for Na_3ScF_6 and K_2NaScF_6 , however, would require critical strains which are greater than those that could be imposed by commercially available perovskite substrates. Nonetheless, we posit that strain stabilization of ferroelectric double perovskites may be experimentally realized with alternate chemistries. For instance similar studies for double perovskites fluorides that substitute Sc^{3+} for the smaller Al^{3+} or Ga^{3+} cations may prove successful in reducing the critical strain value. We hope that this work motivates a resurgence of interest in experimental growth of fluoride films for use in present and future technologies.

ACKNOWLEDGMENTS

This material is based upon work supported by the National Science Foundation under grant no. DMR-1454688. DFT calculations were performed on the high-performance computing facilities available at the Center for Nanoscale Materials (CARBON Cluster) at Argonne National Laboratory, supported by the U.S. DOE, Office of Basic Energy Sciences (BES), DE-AC02-06CH11357, and at the Extreme Science and Engineering Discovery Environment (XSEDE), which is supported by the National Science Foundation grant no. DMR-1100085.

- * neniancharles@drexel.edu
- † jrondinelli@northwestern.edu
- ¹ K. M. Rabe, M. Dawber, C. Lichtensteiger, C. H. Ahn, and J.-M. Triscone, in *Physics of Ferroelectrics, a Modern Perspective*, edited by K. M. Rabe, C. H. Ahn, and J.-M. Triscone (Springer, 2007) pp. 1–30.
 - ² M. W. J. Prins, K. Grosse-Holz, G. Müller, J. F. M. Cillessen, J. B. Giesbers, R. P. Weening, and R. M. Wolf, *Applied Physics Letters* **68**, 3650 (1996).
 - ³ J. F. Scott, *Ferroelectric memories* (Springer-Verlag, 2000).
 - ⁴ M. Lines and A. Glass, *Principles and Applications of Ferroelectrics and Related Materials* (Clarendon, Oxford, 1977).
 - ⁵ P. S. Halasyamani and K. R. Poeppelmeier, *Chemistry of Materials* **10**, 2753 (1998).
 - ⁶ J. W. Bennett and K. M. Rabe, *Journal of Solid State Chemistry* **195**, 21 (2012).
 - ⁷ G. Bergerhoff, I. Brown, F. Allen, *et al.*, International Union of Crystallography, Chester, 77 (1987).
 - ⁸ A. Belsky, M. Hellenbrandt, V. L. Karen, and P. Luksch, *Acta Crystallographica Section B* **58**, 364 (2002).
 - ⁹ H. W. Eng, P. W. Barnes, B. M. Auer, and P. M. Woodward, *Journal of Solid State Chemistry* **175**, 94 (2003).
 - ¹⁰ M. Fornari and D. J. Singh, *Phys. Rev. B* **63**, 092101 (2001).
 - ¹¹ N. A. Benedek and C. J. Fennie, *The Journal of Physical Chemistry C* **117**, 13339 (2013), <http://dx.doi.org/10.1021/jp402046t>.
 - ¹² D. I. Bilec and D. J. Singh, *Physical Review Letters* **96**, 147602 (2006).
 - ¹³ S. V. Halilov, M. Fornari, and D. J. Singh, *Phys. Rev. B* **69**, 174107 (2004).
 - ¹⁴ R. E. Cohen, *Nature* **358**, 136 (1992).
 - ¹⁵ M. Kunz and I. D. Brown, *Journal of Solid State Chemistry* **115**, 395 (1995).
 - ¹⁶ R. G. Pearson, *Journal of Molecular Structure: THEOCHEM* **103**, 25 (1983).
 - ¹⁷ J. F. Scott and R. Blinc, *Journal of Physics: Condensed Matter* **23**, 113202 (2011).
 - ¹⁸ I. Flerov, M. Gorev, A. Tressaud, and N. Laptash, *Crystallography Reports* **56**, 9 (2011).
 - ¹⁹ Z. G. Ye, J. Ravez, J.-P. Rivera, J.-P. Chaminade, and H. Schmid, *Ferroelectrics* **124**, 281 (1991).
 - ²⁰ J. Ravez, *J. Phys. III France* **7**, 1129 (1997).
 - ²¹ We note that the prototypical double perovskite fluorides can be characterized using the same Glazer tilt systems used for perovskite oxides ($a^0a^0a^0$ and $a^-a^-c^+$),^{18,56,57} and that the common tilt pattern observed in orthorhombic perovskite oxides is essentially the same as that for the cryolite fluorides.
 - ²² L. J. Schowalter and R. W. Fathauer, *Journal of Vacuum Science and Technology A* **4**, 1026 (1986).
 - ²³ A. C. Garcia-Castro, N. A. Spaldin, A. H. Romero, and E. Bousquet, *Phys. Rev. B* **89**, 104107 (2014).
 - ²⁴ H. Ishiwara and T. Asano, *Applied Physics Letters* **40**, 66 (1982).
 - ²⁵ T. P. Smith, J. M. Phillips, W. M. Augustyniak, and P. J. Stiles, *Applied Physics Letters* **45**, 907 (1984).
 - ²⁶ J. H. Haeni, P. Irvin, W. Chang, R. Uecker, P. Reiche, Y. L. Li, S. Choudhury, W. Tian, M. E. Hawley, B. Craigo, A. K. Tagantsev, X. Q. Pan, S. K. Streiffer, L. Q. Chen, S. W. Kirchoefer, J. Levy, and D. G. Schlom, *Nature* **430**, 758 (2004).
 - ²⁷ A. Antons, J. B. Neaton, K. M. Rabe, and D. Vanderbilt, *Physical Review B* **71**, 024102 (2005).
 - ²⁸ C.-J. Eklund, C. J. Fennie, and K. M. Rabe, *Physical Review B* **79**, 220101 (2009).
 - ²⁹ V. M. Goldschmidt, *Naturwissenschaften* **14**, 477 (1926).
 - ³⁰ R. D. Shannon and C. T. Prewitt, *Acta Crystallographica Section B* **26**, 1046 (1970).
 - ³¹ S. Carlson, Y. Xu, and R. Norrestam, *Journal of Solid State Chemistry* **135**, 116 (1998).
 - ³² S. Hao, L. Sun, G. Chen, H. Qiu, C. Xu, T. N. Soitah, Y. Sun, and C. Yang, *Journal of Alloys and Compounds* **522**, 74 (2012).
 - ³³ V. Marx, *physica status solidi (b)* **220**, 805 (2000).
 - ³⁴ C. Reber, H. U. Gudel, G. Meyer, T. Schleid, and C. A. Daul, *Inorganic Chemistry* **28**, 3249 (1989), <http://dx.doi.org/10.1021/ic00315a034>.
 - ³⁵ J. P. Perdew, A. Ruzsinszky, G. I. Csonka, O. A. Vydrov, G. E. Scuseria, L. A. Constantin, X. Zhou, and K. Burke, *Phys. Rev. Lett.* **100**, 136406 (2008).
 - ³⁶ G. Kresse and J. Furthmüller, *Phys. Rev. B* **54**, 11169 (1996).
 - ³⁷ G. Kresse and D. Joubert, *Phys. Rev. B* **59**, 1758 (1999).
 - ³⁸ P. E. Blöchl, *Phys. Rev. B* **50**, 17953 (1994).
 - ³⁹ H. J. Monkhorst and J. D. Pack, *Physical Review B* **13**, 5188 (1976).
 - ⁴⁰ A. Togo, F. Oba, and I. Tanaka, *Physical Review B* **78**, 134106 (2008).
 - ⁴¹ See Supplemental Material at [URL will be inserted by publisher] for discussion of the intermediate structure mode decompositions, strain-dependence of the various symmetry-adapted modes, and structure files to visualize the mode displacements.
 - ⁴² For consistency, the mode notation is always specified with reference to the parent $Fm\bar{3}m$ structure.
 - ⁴³ For epitaxial calculations of the monoclinic $P2_1/n$, Pm and Cm phases, we constrain the monoclinic angles $\beta = 90^\circ$ and it is not permitted to relax.
 - ⁴⁴ J. M. Perez-Mato, D. Orobengoa, and M. I. Aroyo, *Acta Crystallographica Section A* **66**, 558 (2010).
 - ⁴⁵ D. G. Schlom, L.-Q. Chen, C.-B. Eom, K. M. Rabe, S. K. Streiffer, and J.-M. Triscone, *Ann. Rev. Mater. Res.* **37**, 589 (2007).
 - ⁴⁶ R. E. Cohen and H. Krakauer, *Phys. Rev. B* **42**, 6416 (1990).
 - ⁴⁷ H. Wang, L. He, and X. Wu, *Computational Materials Science* **96**, Part A, 171 (2015).
 - ⁴⁸ J. M. Rondinelli and N. A. Spaldin, *Advanced Materials* **23**, 3363 (2011).
 - ⁴⁹ J. Íñiguez, M. Stengel, S. Prosandeev, and L. Bellaiche, *Phys. Rev. B* **90**, 220103 (2014).
 - ⁵⁰ D. G. Schlom, L.-Q. Chen, C. J. Fennie, V. Gopalan, D. A. Muller, X. Pan, R. Ramesh, and R. Uecker, *MRS Bulletin* **39**, 118 (2014).
 - ⁵¹ G. Pilania and T. Lookman, *Phys. Rev. B* **90**, 115121 (2014).
 - ⁵² W. Massa and D. Babel, *Chemical Reviews* **88**, 275 (1988).
 - ⁵³ Y. L. Li, S. Choudhury, J. H. Haeni, M. D. Biegalski, A. Vasudevarao, A. Sharan, H. Z. Ma, J. Levy, V. Gopalan, S. Trolier-McKinstry, D. G. Schlom, Q. X. Jia, and L. Q. Chen, *Phys. Rev. B* **73**, 184112 (2006).

- ⁵⁴ A. Vasudevarao, S. Denev, M. D. Biegalski, Y. Li, L.-Q. Chen, S. Trolier-McKinstry, D. G. Schlom, and V. Gopalan, [Applied Physics Letters](#) **92**, 192902 (2008).
- ⁵⁵ I. D. Brown and K. R. Poeppelmeier, *Bond Valences*, Vol. 158 (Springer, 2014).
- ⁵⁶ I. Flerov, M. Gorev, K. Aleksandrov, A. Tressaud, J. Grannec, and M. Couzi, [Materials Science and Engineering: R: Reports](#) **24**, 81 (1998).
- ⁵⁷ I. Flerov, M. Gorev, K. Aleksandrov, A. Tressaud, and V. Fokina, *Crystallography Reports* **49**, 100 (2004).